High-harmonic fast magnetosonic wave coupling, propagation, and heating in a spherical torus plasma*

J. Menard,† R. Majeski, R. Kaita, M. Ono, and T. Munsat
Princeton Plasma Physics Laboratory, Princeton, New Jersey 08543

D. Stutman and M. Finkenthal
Johns Hopkins University, Baltimore, Maryland 21205

(Received 16 November 1998; accepted 18 February 1999)

A novel rotatable two-strap antenna has been installed in the current drive experiment upgrade (CDX-U) [T. Jones, Ph.D. thesis, Princeton University (1995)] in order to investigate high-harmonic fast wave coupling, propagation, and electron heating as a function of strap angle and strap phasing in a spherical torus plasma. Radio-frequency-driven sheath effects are found to fit antenna loading trends at very low power and become negligible above a few kilowatts. At sufficiently high power, the measured coupling efficiency as a function of strap angle is found to agree favorably with cold plasma wave theory. Far-forward microwave scattering from wave-induced density fluctuations in the plasma core tracks the predicted fast wave loading as the antenna is rotated. Signs of electron heating during rf power injection have been observed in CDX-U with central Thomson scattering, impurity ion spectroscopy, and Langmuir probes. While these initial results appear promising, damping of the fast wave on thermal ions at high ion-cyclotron-harmonic number may compete with electron damping at sufficiently high ion β—possibly resulting in a significantly reduced current drive efficiency and production of a fast ion population. Preliminary results from ray-tracing calculations which include these ion damping effects are presented. © *1999 American Institute of Physics.* [S1070-664X(99)97305-6]

I. INTRODUCTION

Spherical torus (ST) plasmas[1] have received considerable attention recently due primarily to encouraging magnetohydrodynamic (MHD) stability results from the small tight aspect ratio tokamak (START) experiment[2,3] and promising theoretical predictions regarding stability[4–6] and confinement.[7] However, the compact geometry of the ST greatly limits the inductive heating and current drive capability of the ohmic heating solenoid. Further, to maximize the space available for toroidal field conductors in the center column, the ohmic heating solenoid should ideally be absent. Thus, the development of noninductive plasma start-up, heating, and current drive methods is essential if the ST is to be a net power producing device.[8]

In this regard, fast magnetosonic waves are predicted to damp strongly on electrons in the high-β plasma[9] of next-generation ST devices such as the national spherical torus experiment (NSTX)[10] and the mega amp spherical tokamak (MAST)[11] and should be capable of generating significant plasma current. The idea of using fast waves to heat electrons via Landau and transit-time damping is not new,[12] and the theory of electron heating and current drive using fast waves is well developed for standard tokamak plasmas.[13] However, experimental verification of the feasibility of generating direct fast wave electron heating and current drive in a tokamak plasma is relatively recent. Several early experiments required the generation of a fast electron population for the wave to damp on[14,15] and required a careful choice of plasma parameters[16,17] to eliminate slow wave propagation and slow wave current drive. Fast wave experiments on the DIII-D tokamak have shown that with a careful choice of wave parameters, optimal launch spectrum, and wall conditioning via boronization, nearly 100% of the incident fast wave power can be absorbed by electrons.[18] Importantly, nearly all of these fast wave experiments were constrained to $\omega_{\mathrm{pe}}/\Omega_e \approx 1$.

To better understand the meaning of this constraint, it can be shown (see, for example, Ref. 13) that the inverse perpendicular electron damping length of the fast wave is proportional to $k_{\perp r}\beta_e\xi_e e^{-\xi_e^2}$. Here $k_{\perp r} \approx \omega_{\mathrm{rf}}/v_A$, $v_A \approx c(\Omega_i/\omega_{\mathrm{pi}})$, $\beta_e = 2\mu_0 n_e T_e/B^2$, $\xi_e = \omega/k_\parallel V_{Te}$, and $V_{Te} = \sqrt{2T_e/m_e}$. The relative phase velocity ξ_e is typically chosen by antenna phasing (launched $k_\parallel$) to maximize either heating or current drive efficiency, so the inverse damping length scales roughly as $(\omega_{\mathrm{pe}}/\Omega_e)^3 T_e$. From this relation it is immediately obvious why additional electron heating (or tail formation) is often used to increase wave damping.

As discussed in Ref. 9, the feature of a high-β plasma most relevant to fast wave damping is the relatively low magnetic field or, equivalently, large perpendicular permittivity $\epsilon_\perp \approx (\omega_{\mathrm{pe}}/\Omega_e)^2$ and slow Alfvén speed v_A. For the expected NSTX plasma parameters of $n_e = 5\times 10^{19}\ \mathrm{m}^{-3}$ and $B = 0.3$ T, $\omega_{\mathrm{pe}}/\Omega_e \approx 7$. Thus, in a ST plasma, fast waves at high harmonics of the ion cyclotron frequency may damp so strongly on electrons that efficient off-axis current drive and current profile control might be possible provided that para-

*Paper H4I1.4 Bull. Am. Phys. Soc. **43**, 1773 (1998).
†Invited speaker.

 © 1999 American Institute of Physics

sitic ion damping at cyclotron harmonics is sufficiently weak.

Another unique feature of ST plasmas relevant to wave excitation and propagation is the strong field line tilt and shear at the outboard side of the plasma. The magnitude and potential variability of this tilt during a plasma discharge could complicate coupling to the fast wave. To address such coupling issues and attempt to observe electron heating using high frequency fast waves, a two strap antenna with arbitrary strap phasing was installed in the current drive experiment upgrade (CDX-U) spherical torus.[19] The novel feature of this antenna is that it is manually rotatable between plasma discharges. In this paper, we report on recent experimental and theoretical investigations of high frequency fast wave coupling and heating physics as a function of the angle between the antenna current straps and the edge magnetic field.[20]

The remainder of this article is organized as follows: a description of the experimental apparatus used during the CDX-U experiments is described in Sec. II. Systematic measurements of plasma loading are described in Sec. III. Measurements of internal rf wave fields obtained using far-forward microwave scattering are discussed in Sec. IV. Observations of electron temperature increases during high-harmonic fast wave (HHFW) excitation are discussed in Sec. V. Ray-tracing calculations incorporating the effect of power absorption by thermal ions at high ion-cyclotron-harmonic number are discussed in Sec. VI. Finally, a summary of these results is given in Sec. VII.

II. EXPERIMENTAL APPARATUS

CDX-U is a low-aspect-ratio tokamak facility with $R_0 \approx 35$ cm, $A = R_0/a \geqslant 1.5$, $\kappa = b/a \approx 1.5$, $B_{t0} \leqslant 1.2$ kG, and $I_P = 50-80$ kA. The total discharge pulse length is roughly 20 ms with a flattop duration of approximately 5 ms. The peak central electron density is typically $0.5-2\times10^{13}$ cm^{-3}, the line-averaged density is $2-4\times10^{12}$ cm^{-3}, and $T_e(0)\approx100$ eV. A drawing of the device is shown in Fig. 1.

The CDX-U rotatable HHFW antenna is capable of coupling several hundred kilowatts to the plasma (for typical loading values) for pulse durations of $\leqslant 10$ ms. The strap height, width, and center-to-center separation are approximately 27, 3.8, and 22 cm, respectively. The strap separation was chosen to launch toroidal mode number $n_\phi \approx 8$ with 0°–180° phasing. Each antenna strap is surrounded by four 0.635 cm thick boron nitride insulating limiter plates to minimize radio-frequency sheath effects.[21] More details of the CDX-U antenna can be found in Ref. 20. For all data below, either hydrogen or deuterium plasmas were used, and the antenna frequency was 12 MHz corresponding to $\omega/\Omega_{\mathrm{H}} \approx 8$ and $\omega/\Omega_{\mathrm{D}} \approx 16$ at the antenna.

III. PLASMA LOADING

One of the first measurements made with the HHFW antenna was of antenna loading resistance. In the discussions that follow, the strap loading resistance, R_{STRAP}, is defined as the effective resistance of each strap such that the power into each strap is conserved, since the strap input power and circulating current are measured quantities. The plasma loading resistance, R_{PLASMA}, is defined as the difference between R_{STRAP} and the intrinsic resistance of each strap in vacuum. Systematic measurements of plasma loading resistance as a function of input power, strap angle, and relative strap phasing provide insight into the mechanisms which dissipate antenna input power.

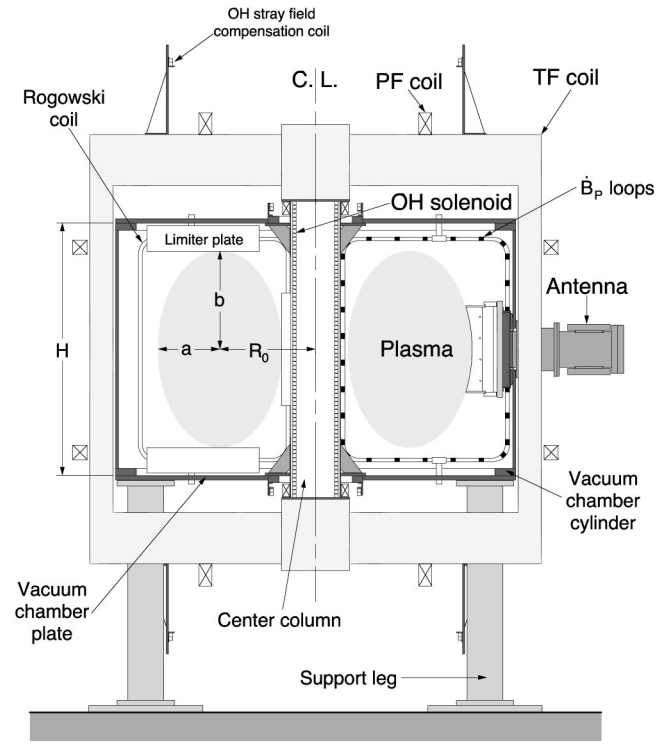

FIG. 1. Layout of the CDX-U device, December 1997.

A. Loading as a function of power

Early measurements of plasma loading resistance found that loading was largest at very low power levels and asymptotically approached a constant value above a few kW. Loading due to the radiation of waves is expected to be independent of power since power flux out of the antenna is proportional to the square of the wave electric field (strap current). One mechanism which can introduce power-dependent loading is ponderomotive density expulsion in front of the antenna.[22,23] In principle, density expulsion could explain the loading drop observed in the CDX-U experiments by reducing the fast wave coupling efficiency as the power is increased. Ponderomotive density expulsion was invoked to explain poor coupling to the ion Bernstein wave (IBW) in DIII-D,[24] and more recent experiments[23,25] and theory[26] convincingly show that such effects can be important. For CDX-U parameters $T_e = 15$ eV (edge) and f=12 MHz, the smallest wave electric field at which such perturbations will appear is given approximately by (mks)

$$E > \left[\frac{2 m_e \omega^2 k_B T_e}{e^2}\right]^{1/2} \approx 1 \text{ kV/m}. \tag{1}$$

Taking the inductive electric field along the strap as an upper limit on the electric field at the plasma surface, the above inequality implies that ponderomotive effects might begin to

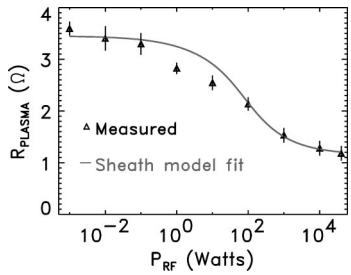

FIG. 2. Plasma loading resistance vs coupled rf input power for vertical straps and 0°–90° strap phasing in hydrogen.

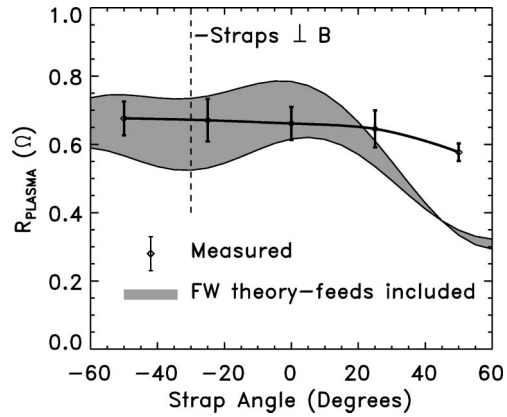

FIG. 3. Plasma loading resistance vs antenna strap angle for 0°–180° strap phasing and $P_{rf}=50-70$ kW in hydrogen. Note that straps are perpendicular to **B** at −30°.

become important above the 1 kW power level. Since the loading is already nearly constant above this power level, ponderomotive effects cannot explain the observed loading.

In addition to the observed loading resistance becoming constant at high power, signs of saturation in the loading resistance at sufficiently low power were also observed. Both trends are consistent with power dissipation in rf-driven sheaths.[27–31] Insight into how rf sheath dissipation should scale with plasma and antenna parameters can be gained from an analytic model of an rf-driven plasma-filled parallel plate capacitor.[31] One prediction of this model is that the rf induced change in plasma potential on field lines linking the antenna to ground should scale quadratically with oscillating strap current (I_{STRAP}) rather than linearly if the strap current is made sufficiently small. Since the incremental power dissipated in sheaths (by ions) should scale as the product of the ion saturation current and change in plasma potential, the predicted parasitic loading caused by sheath dissipation, R_{SH}, should tend to a constant value as $\xi \equiv eV_{\mathrm{rf}}/T_e \rightarrow 0$. Here V_{rf} is a voltage proportional to the strap current. The scaling for arbitrary ξ derived in Ref. 31 is

$$R_{\mathrm{SH}}(\xi) \approx R_{\mathrm{SH}}^{\xi=0} \frac{1+0.6\xi}{1+\xi} \frac{2I_1(\xi)}{\xi I_0(\xi)}, \tag{2}$$

where I_0 and I_1 are modified Bessel functions.

Figure 2 shows the loading resistance measured over nearly eight orders of magnitude in coupled rf input power (using three different amplifiers) compared to the sheath model assuming $R_{\mathrm{SH}}^{\xi=0} \approx 2\Omega$, $V_{\mathrm{rf}} \approx 6\Omega \times I_{\mathrm{STRAP}}$, and an asymptotic loading value of 1.2 Ω. As seen in the figure, this three parameter model provides a good fit to the data, although the change in slope in the theoretical curve in the 1–10 W power range is somewhat more rapid than experimentally measured. From this fit, V_{rf} is estimated to be approximately 20%–40% of the inductive voltage drop along the length of the strap.

B. High-power loading as a function of antenna angle

In general, plasma loading was observed to decrease as the antenna straps became parallel to **B** (although sometimes only weakly). This behavior is consistent with fast wave excitation, since the fast wave is predominantly a compressional wave. Further, the strap phasing which launches the largest parallel wave number (i.e., 0°–180° strap phasing) exhibited the smallest loading of any phasing. This is also consistent with fast wave excitation since high parallel wave number wave fields not only decay more rapidly at the plasma edge, but also must tunnel through a larger cutoff distance at the plasma edge before they begin to propagate. Cold plasma slow waves are strongly evanescent for these plasma parameters and direct IBW excitation should be weak,[32] so fast wave radiation should be the dominant source of loading if sheath dissipation is comparatively small at high power. The sheath loading analysis of the preceding section indicates that less than 5% of total input power is dissipated in sheaths for input powers above 50 kW. The lack of any significant antenna-plasma interaction at these power levels regardless of antenna angle and phasing is presumably due to the use of insulating limiter plates.

Figure 3 compares the measured plasma loading as a function of antenna angle for 0°–180° strap phasing to that predicted by a cold-plasma coupling code written specifically for these ST experiments.[20] As seen in the figure, good agreement is obtained between experiment and theory so long as the straps are not too nearly parallel to **B**. Density and magnetic field profiles derived from equilibrium reconstructions were used in the coupling simulations, field-line pitch and shear effects were found to be important, and all relevant $1/R$ effects are included in the equations for the fast wave fields in front of the antenna. The uncertainty in the predicted loading is due primarily to the uncertainty in the absolute magnitude of the electron density which was measured using a triple Langmuir probe.[33] Without the inclusion of the tangential electromagnetic fields from the strap feeds in the modeling,[34] the predicted loading is four times larger than measured. The antenna is modeled without a Faraday shield, as earlier coupling simulations with an ideal shield included[35] predicted unrealistically large loading values for strap angles nonorthogonal to **B**.

IV. MICROWAVE SCATTERING MEASUREMENTS

To better understand fast wave coupling and propagation physics in CDX-U, the vertical beam of the CDX-U 2 mm interferometer[36] has been used to measure far-forward microwave scattering off of electron density fluctuations induced by rf wave fields in the plasma. The interferometer

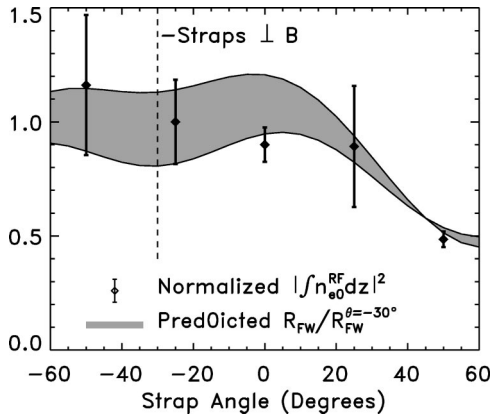

FIG. 4. The square of the 12 MHz scattering signal at fixed strap current (500 A_{p-p}) compared to the predicted fast wave loading resistance both renormalized to their respective values at −30° strap angle. Data taken in hydrogen with 0°–180° strap phasing.

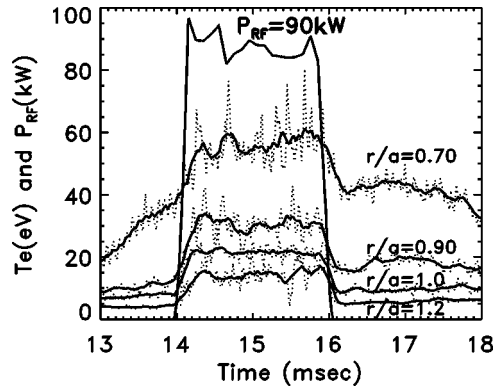

FIG. 5. Electron temperature measured with a triple Langmuir probe at several major-radial locations in the outer part of the CDX-U plasma. Dotted lines represent raw data, solid lines the raw data smoothed over several MHD periods. Data taken in hydrogen with vertical straps and 0°–180° phasing.

beam is located 90° away from the antenna toroidally, and should therefore be relatively unaffected by antenna near fields. The beam major radius can be varied from a few centimeters inside the magnetic axis to the edge of the plasma, but scattered signals are typically quite weak outside $r/a=0.5$. One fortunate side effect (with regard to the scattering experiments) of these MHD active plasmas is the peaking of the electron density profile. This peaking causes the scattered signal to be dominated by scattering from the core, and therefore allows accurate measurement of variations in the core wave field amplitude as antenna parameters are changed.

Under the above conditions, the core wave-field energy density should be approximately proportional to $|\int n_{e0}^{\mathrm{rf}}(z)dz|^2$ where $\int n_{e0}^{\mathrm{rf}}(z)dz$ is the 12 MHz line-integrated electron density fluctuation amplitude. For fixed strap current, the power radiated into the fast wave should be proportional to the radiation resistance of the fast wave. Assuming the fast wave damping rate is constant during the short ($\Delta t \leqslant 500$ μs) scattering measurement, the wave-field energy density (at fixed strap current) and fast wave radiation resistance should therefore be linearly related. A comparison between the scattered signal amplitude and the theoretically predicted fast wave loading as a function of strap angle is shown in Fig. 4. The scattering data are taken with the beam passing through the magnetic axis and both curves are normalized to their respective values when the straps are orthogonal to **B**. As seen in the figure, both curves show a very similar dependence on strap angle, and together imply that most of the rf input power is radiated into the fast wave until the straps become nearly parallel to **B**. When the straps are parallel to **B**, half of the input power is apparently dissipated by some means other than (cold plasma) fast wave radiation.

V. ELECTRON HEATING

With antenna limiter bakeout and steady-state titanium sublimation gettering, increases in carbon and oxygen line radiation consume no more than 20% of the coupled rf input power ($\leqslant$100 kW) even when the straps are parallel to the edge equilibrium **B**. In such discharges, rf electron heating has been observed in hydrogen and deuterium plasmas using a triple Langmuir probe, carbon V (CV) spectroscopy, and central Thomson scattering. Unfortunately, however, the central Thomson scattering diagnostic was not available during many of the rf heating experiments. The characteristic *e*-folding times of the rise and decay phases of the electron temperature increase during rf (measured using the triple probe) are consistent with the global energy confinement time (80–100 μs) of these MHD-active plasmas,[19] and energy balance calculations using this confinement time and the measured increases in radiated power and electron stored energy find that 50%–80% of the rf input power can be accounted for. The electron density rise (line-integrated) during rf heating is typically less than 10%.

One of the more surprising findings from both central Thomson scattering and CV spectroscopy measurements was that the central electron temperature increase during rf was persistently smaller than expected. Typical central electron temperature increases during rf were in the range of 10–15 eV, and similar increases were measured in the outer regions of the plasma. Heating outside the core of the plasma is evident in Fig. 5 which shows the electron temperature measured using a triple Langmuir probe located 10° away from the antenna toroidally at a normalized minor radius $r/a \geqslant 0.6$ on the equatorial midplane. In contrast, Fig. 6 shows the predicted power deposition profiles computed using both fast wave ray tracing[37] based on the hot-electron dispersion relation derived in Ref. 9 and the toroidal ion cyclotron (TORIC) full-wave code.[38] Clearly, the measured profile of electron heating is apparently much broader than predicted by either code.

One possible explanation of this discrepancy is that collisionless electron heating in the antenna near field[39] is competitive with linear Landau damping in the plasma core. Such nonlinear effects are not included in either of the aforementioned codes. Another possibility is that since the pre-rf central electron temperature is typically just below 100 eV, most of the core rf power is consumed through impurity ionization and radiation rather than increases in electron stored energy. While most rf heated discharges have not

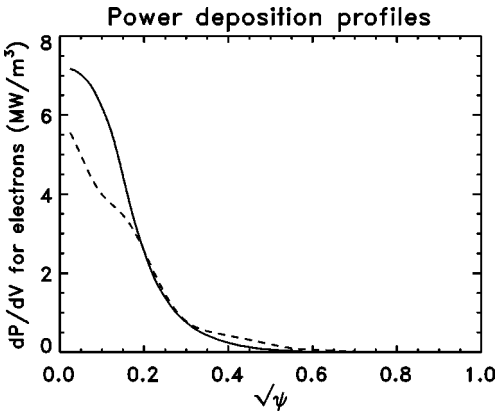

FIG. 6. Predicted power deposition profiles for electron heating in CDX-U computed using hot-electron ray tracing (solid line) and the TORIC full-wave code (dashed line) for an rf input power of 100 kW.

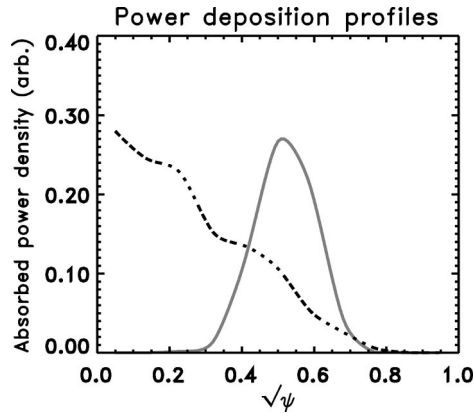

FIG. 7. Predicted power deposition profiles for NSTX using cold-ion ray tracing for the equilibrium of Sec. VI and a launched toroidal mode number $n_\phi = 6$. The solid line includes the full equilibrium magnetic field, while the equilibrium poloidal field has been reduced by 90% for the dashed curve.

shown dramatic core electron temperature increases, there are a few cases which show as much as a 50% increase in T_e in the core. For such cases, the measured electron heating profile more closely resembles the theoretical predictions. Much of the supporting analysis for these findings can be found in Ref. 40, and this reference also discusses how the rapid radial transport in the low-field CDX-U device may lead to a core impurity accumulation instability[41] which would make large increases in core electron temperature difficult to produce at the rf power levels used in these experiments.

VI. PREDICTIONS FOR NSTX

The NSTX device will initially utilize a HHFW antenna capable of delivering 6 MW of 30 MHz rf power as its primary auxiliary heating system until its neutral beam injection system becomes operational. The antenna is comprised of 12 toroidally phased straps oriented vertically (poloidally) which cover 90° in toroidal angle on the outboard midplane. Similar to the CDX-U antenna, each approximately 1 m tall strap will have its own Faraday shield and boron nitride insulating plates separating adjacent straps to minimize rf-sheath formation. Given the successful coupling to the fast wave measured on CDX-U even with large strap-field misalignment angles, it is anticipated that the NSTX antenna will also efficiently couple to the fast wave even when the edge poloidal field is similar in magnitude to the toroidal field.

Given the thorough WKB analysis originally performed in Ref. 9 and the more recent one-dimensional (1D) full-wave analysis described in Ref. 42, there seems to be little doubt theoretically that high-harmonic fast waves can efficiently heat electrons. Both of the aforementioned articles also find that ion-cyclotron-harmonic damping can become important if the ion temperature is sufficiently large. Quantifying the power absorbed by the ions is difficult, however, without including both a realistic equilibrium magnetic field and understanding how these equilibrium effects can alter the fast wave power flow. The purpose of the following analysis is to show briefly how the poloidal magnetic field can alter the power deposition profile of the fast wave and correspondingly impact the fraction of power absorbed by thermal ions.

Given the short perpendicular wavelength of the fast wave in NSTX plasmas and the dearth of two-dimensional (2D) toroidal full wave codes capable of treating waves with $(k_\perp \rho_i)^2 \gg 1$, ray tracing is a useful analysis tool for the present problem. Ray tracing is performed using the hot-electron (cold-ion) dispersion relation from Ref. 9 to determine the power flow trajectory and $n_\parallel$ evolution. The full hot plasma dispersion relation is then solved using the cold-ion $n_\parallel$ and equilibrium quantities along the ray trajectory to obtain the exact electric field polarization and electron and ion absorption within the WKB approximation. As discussed in Ref. 42, the electron and ion kinetic fluxes must be properly accounted for to obtain positive definite absorption. The ray tracing code is interfaced with J-SOLVER[43] equilibrium solutions to include a realistic equilibrium magnetic field.

The reference NSTX equilibrium under consideration is taken from Fig. 6 of Ref. 4 and has a vacuum toroidal magnetic field at the plasma geometric center of 0.3 T and a plasma current of 1.1 MA. The central electron and deuterium densities are taken to be 3.8×10^{13} cm^{-3}, the central electron temperature is held fixed at 1.5 keV, and the deuterium temperature (T_D) is varied to determine ion damping as a function of T_D. The density and temperature profiles are assumed to be broad, and the strong poloidal field typical of such equilibria helps to form an absolute magnetic well on the low-field side of the plasma.

The effect of this strong poloidal field on power flow and damping is illustrated in Fig. 7 for a launched toroidal mode number $n_\phi = 6$. The solid curve in the figure includes the full equilibrium poloidal field, while the dashed curve has the poloidal magnetic field artificially reduced by 90%. In both cases, the group velocity (power flow) has a significant component parallel to the equilibrium magnetic field, and in the case with the full poloidal field, the power flow develops a significant vertical (as opposed to purely major radial and toroidal) component. Further, the poloidal magnetic field causes the parallel wave vector to upshift much more rapidly

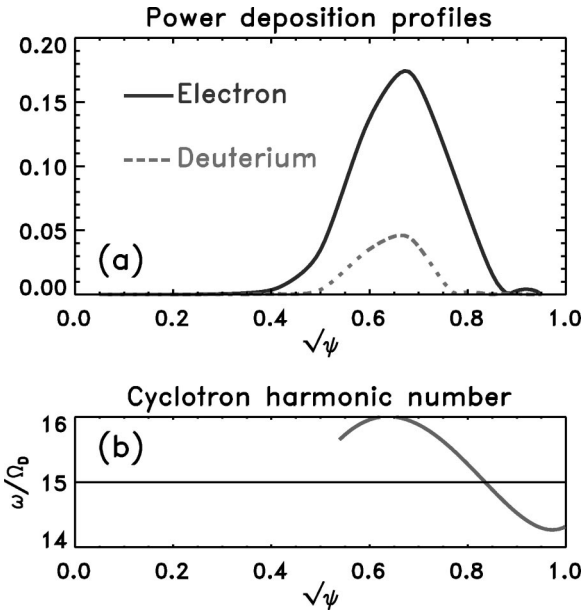

FIG. 8. Predicted power deposition profiles for NSTX with $T_e(0)=1.5$ keV and $T_D(0)=1$ keV for the equilibrium of Sec. VI and a launched toroidal mode number $n_\phi=12$.

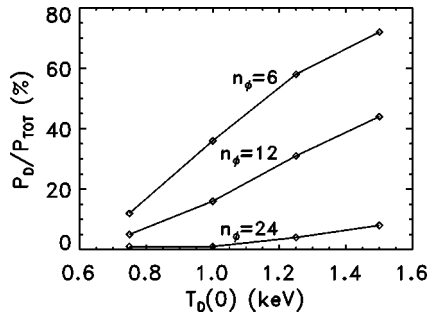

FIG. 9. Predicted fraction of power absorbed by deuterium ions as a function of central deuterium temperature and launched toroidal mode number in NSTX.

than $1/R$. These effects, combined with the fact that the single pass absorption is already approaching 100%, lead to power deposition profiles which are relatively narrow and typically localized off axis. At higher launched n_ϕ (higher $n_\parallel$), the fast wave damps off axis regardless of the poloidal magnetic field strength. For the CDX-U experiments discussed in Sec. V, the predicted power deposition profile is peaked on axis despite the strong poloidal field because the single-pass absorption is less than 10%.

While these effects are perhaps not surprising, they are important with regard to ion damping because the ray trajectory determines how many ion-cyclotron resonances are encountered as the power is deposited, and the parallel wave number and local ion temperature determine the width of each resonance. Figure 8(a) shows power deposition profiles for damping on electrons and deuterium ions for a central deuterium temperature of 1 keV and a launched $n_\phi=12$. As seen in Fig. 8(b), the ray passes through two cyclotron resonances as it completely damps, and nearly all of the ion damping occurs at the 16th harmonic. For this particular set of parameters, 16% of the fast wave power is predicted to be absorbed by thermal deuterium ions. Figure 9 summarizes the deuterium power absorption fraction for a range of ion temperatures and launched n_ϕ. As seen in the figure, the absorbed fraction increases rapidly with increasing temperature above 750 eV, and low n_ϕ absorbs the most power at fixed ion temperature. For $n_\phi<4$ and $T_D>1$ keV, the ion Bernstein root begins to coalesce with the fast wave root, and the damping results become suspect. Launching high n_ϕ appears to be one way to significantly reduce the ion damping. Lastly, careful adjustment of the equilibrium (or wave frequency) to launch power between edge harmonics can reduce the ion absorption by roughly a factor of 2, but such tailoring may be difficult experimentally.

VII. SUMMARY AND CONCLUSIONS

A novel rotatable two-strap antenna has been installed in the current drive experiment upgrade (CDX-U) in order to investigate HHFW coupling, propagation, and electron heating as a function of strap angle and strap phasing in a ST plasma. rf-driven sheaths appear to be responsible for increases in antenna loading at very low power levels, but the loading attributable to this effect becomes negligible above a few kilowatts for all strap angles and phasings tested. Boron nitride insulating limiter plates, while apparently not completely eliminating sheath effects, appear to eliminate any strongly deleterious antenna-plasma interaction local to the antenna.

At sufficiently high power, i.e., once the loading has become independent of power, the measured coupling efficiency as a function of strap angle is found to agree favorably with cold plasma wave theory until the straps become nearly parallel to the equilibrium magnetic field. When the straps are parallel to the field, half of the coupled input power cannot be accounted for. Far-forward microwave scattering from wave-induced density fluctuations in the plasma core indicates that using cold plasma theory to model fast wave excitation is a good approximation for CDX-U plasmas, as the predicted fast wave loading and scattering signal show a very similar dependence on strap angle as the antenna is rotated. Signs of electron heating during rf power injection have been observed in CDX-U with central Thomson scattering, impurity ion spectroscopy, and Langmuir probes. The central electron temperature increase is typically not as large as predicted by standard rf wave heating theory. However, 50%–80% of the rf input power can be accounted for in both hydrogen and deuterium plasmas provided the antenna and vacuum chamber are properly conditioned.

While these initial results appear promising with regard to efficiently coupling to the fast wave and heating electrons in NSTX, damping of the fast wave on thermal ions at high ion-cyclotron-harmonic number may compete with electron damping at sufficiently high ion β. The present WKB analysis of the ion power absorption predicts that ion heating may become non-negligible above 1 keV central ion temperature for typical NSTX plasma parameters and should be strongly dependent on antenna strap phasing. It must be stated, however, that while the WKB approximation appears to be well satisfied in the region where the power is absorbed by the

ions (and electrons), the present analysis completely ignores, among other things, trapped-particle effects which can significantly impact the ion power absorption. These issues and extensions of the hot-plasma ray-tracing model are topics for future research.

ACKNOWLEDGMENTS

Special thanks to Dr. R. Nazikian for his assistance with the microwave scattering measurements and to Dr. T. Seki for his careful calibration of several rf diagnostics. This work was supported by the United States Department of Energy under Contract No. DEAC02-76CHO3037 at the Princeton Plasma Physics Laboratory and by Grant No. DE-FG02-86ER52314AT at Johns Hopkins University.

[1] Y.-K. M. Peng and D. J. Strickler, Nucl. Fusion **26**, 769 (1986).
[2] M. Gryaznevich, R. Akers, P. G. Carolan, N. J. Conway, D. Gates, A. R. Field, T. C. Hender, I. Jenkins, R. Martin, M. P. S. Nightingale, C. Ribeiro, D. C. Robinson, A. Sykes, M. Tournianski, M. Valovi, and M. J. Walsh, Phys. Rev. Lett. **80**, 3972 (1998).
[3] D. A. Gates, R. Akers, L. Appel, P. G. Carolan, N. Conway, J. Dowling, M. Gryaznevich, T. Hender, O. J. Kwon, R. Martin, M. Nightingale, M. Price, C. Roach, A. Sykes, M. R. Tournianski, M. Walsh, C. D. Warrick, S. Team, and N. Team, Phys. Plasmas **5**, 1775 (1998).
[4] J. E. Menard, S. C. Jardin, S. M. Kaye, C. E. Kessel, and J. Manickam, Nucl. Fusion **37**, 595 (1997).
[5] R. L. Miller, Y. R. Lin-Liu, A. D. Turnbull, V. S. Chan, L. D. Perlstein, O. Sauter, and L. Villard, Phys. Plasmas **4**, 1062 (1997).
[6] S. E. Kruger, C. C. Hegna, and J. D. Callen, Phys. Plasmas **5**, 455 (1998).
[7] G. Rewoldt, W. M. Tang, S. Kaye, and J. Menard, Phys. Plasmas **3**, 1667 (1996).
[8] R. D. Stambaugh, V. S. Chan, R. L. Miller, and M. J. Schaffer, Fusion Technol. **33**, 1 (1998).
[9] M. Ono, Phys. Plasmas **2**, 4075 (1995).
[10] J. Spitzer, M. Ono, Y.-K. M. Peng, D. Bashore, T. Bigelow, A. Brooks, J. Chrzanowski, H. M. Fan, P. Heitzenroeder, T. Jarboe, R. Kaita, S. Kaye, H. Kugel, R. Majeski, C. Neumeyer, R. Parsells, E. Perry, N. Pomphrey, J. Robinson, D. Strickler, and R. Wilson, Fusion Technol. **30**, 1337 (1996).
[11] A. C. Darke, M. Cox, J. R. Harbar, J. H. Hay, J. B. Hicks, J. W. Hill, D. Hurford, J. S. McKenzie, A. W. Morris, M. P. S. Nightingale, T. N. Todd, G. M. Voss, and J. R. Watkins, The mega amp spherical tokamak, in *Symposium on Fusion Engineering '95: Seeking a New Energy Era, 16th Symposium on Fusion Engineering*, Champaign, IL, 1995 (Institute of Electrical and Electronics Engineers, Piscataway, NJ, 1995), Vol. 2, p. 1456.
[12] T. H. Stix, Nucl. Fusion **15**, 737 (1975).
[13] S. C. Chiu, V. S. Chan, R. W. Harvey, and M. Porkolab, Nucl. Fusion **29**, 2175 (1989).
[14] J. Goree, M. Ono, P. Colestock, R. Horton, D. McNeill, and H. Park, Phys. Rev. Lett. **55**, 1669 (1985).
[15] T. Yamamoto, Y. Uesugi, H. Kawashima, K. Hoshino, H. Aikawa, S. Kasai, T. Kawakami, T. Kondoh, H. Maeda, T. Matsuda, H. Matsumoto, Y. Miura, M. Mori, K. Odajima, H. Ogawa, T. Ogawa, K. Ohasa, H. Ohtsuka, S. Sengoku, T. Shoji, N. Suzuki, H. Tamai, T. Yamauchi, and I. Nakazawa, Phys. Rev. Lett. **63**, 1148 (1989).
[16] K. Ohkubo, Y. Hamada, Y. Ogawa, A. Mohri, R. Akiyama, R. Ando, S. Hirokura, E. Kako, K. Kawahata, Y. Kawasumi, K. Masai, K. Matsuoka, M. Mugishima, N. Noda, M. Sasao, K. N. Sato, S. Tanahashi, Y. Taniguchi, and K. Toi, Phys. Rev. Lett. **56**, 2040 (1986).
[17] R. Ando, E. Kako, Y. Ogawa, and T. Watari, Nucl. Fusion **26**, 1619 (1986).
[18] C. C. Petty, R. I. Pinsker, M. J. Mayberry, M. Porkolab, F. W. Baity, P. T. Bonoli, S. C. Chiu, J. C. M. de Haas, R. H. Goulding, D. J. Hoffman, T. C. Luce, and R. Prater, Phys. Rev. Lett. **69**, 289 (1992).
[19] T. G. Jones Ph.D. thesis, Princeton University, 1995.
[20] J. E. Menard, Ph.D. thesis, Princeton University, 1998.
[21] R. Majeski, P. H. Probert, T. Tanaka, D. Diebold, R. Bruen, M. Doczy, R. Fonck, N. Hershkowitz, T. Intrator, G. McKee, P. Nonn, J. Pew, and J. Sorensen, Fusion Eng. Des. **24**, 159 (1994).
[22] G. J. Morales and Y. C. Lee, Phys. Rev. Lett. **35**, 930 (1975).
[23] C. Riccardi, M. Fontanesi, A. Penso, and E. Sindoni, Phys. Lett. A **208**, 223 (1995).
[24] M. J. Mayberry, R. I. Pinsker, C. C. Petty, M. Porkolab, S. C. Chiu, W. P. Cary, and R. Prater, Nucl. Fusion **33**, 627 (1993).
[25] G. R. Hanson, C. E. Bush, J. B. Wilgen, T. S. Bigelow, J. H. Rogers, and J. R. Wilson, Measurements of edge density profile modification during IBW on TFTR, in *Radio Frequency Power in Plasmas: 12th Topical Conference*, AIP Conf. Proc. No. 403, Savannah, GA, 1997 (American Institute of Physics, New York, 1997), p. 451.
[26] D. A. Russell, J. R. Myra, and D. A. D'Ippolito, Phys. Plasmas **5**, 743 (1998).
[27] H. S. Butler and G. S. Kino, Phys. Fluids **6**, 1346 (1963).
[28] F. W. Perkins, Nucl. Fusion **29**, 583 (1989).
[29] D. A. D'Ippolito, J. R. Myra, M. Bures, and J. Jacquinot, Plasma Phys. Controlled Fusion **33**, 607 (1991).
[30] J. Sorensen, D. A. Diebold, R. Majeski, and N. Hershkowitz, Nucl. Fusion **33**, 915 (1993).
[31] D. A. D'Ippolito and J. R. Myra, Phys. Plasmas **3**, 420 (1996).
[32] M. Brambilla and A. Cardinali, Nucl. Fusion **32**, 465 (1992).
[33] S.-L. Chen and T. Sekiguchi, J. Appl. Phys. **36**, 2363 (1965).
[34] V. L. Vdovin, Nucl. Fusion **23**, 1435 (1983).
[35] M. Brambilla, Nucl. Fusion **28**, 549 (1988).
[36] C. B. Forest, G. Greene, and M. Ono, Rev. Sci. Instrum. **61**, 2888 (1990).
[37] J. Menard, R. Majeski, M. Ono, and J. R. Wilson, High ion-harmonics fast wave heating in NSTX and CDX-U, in *Proceedings From the 11th Topical Conference on Radio Frequency Power in Plasmas*, AIP Conf. Proc. No. 355, Palm Springs, CA, 1995 (American Institute of Physics, New York, 1995), p. 59.
[38] M. Brambilla, Plasma Phys. Controlled Fusion **41**, 1 (1999).
[39] G. G. Borg, J. Bright, and I. V. Kamenski, Plasma Phys. Controlled Fusion **40**, 987 (1998).
[40] D. Stutman, M. Finkenthal, V. Soukhanovskii, J. Menard, T. Munsat, R. Kaita, and R. Majeski, Plasma Phys. Controlled Fusion (submitted).
[41] M. Z. Tokar, J. Rapp, G. Bertschinger, L. Könen, H. R. Koslowski, A. Krämer-Flecken, V. Philipps, U. Samm, and B. Unterberg, Nucl. Fusion **37**, 1691 (1997).
[42] C. N. Lashmore-Davies, V. Fuchs, and R. A. Cairns, Phys. Plasmas **5**, 2284 (1998).
[43] J. Delucia, S. C. Jardin, and A. M. M. Todd, J. Comput. Phys. **37**, 183 (1980).